Bcl-xL knockout attenuates mitochondrial respiration and causes oxidative stress that is compensated by pentose phosphate pathway activity

Pfeiffer, Annika; Schneider, Julia; Bueno, Diones; Dolga, Amalia; Voss, Timo-Daniel; Lewerenz, Jan; Wüllner, Verena; Methner, Axel

Published in:
Free Radical Biology and Medicine

DOI:
10.1016/j.freeradbiomed.2017.08.007

Publication date:
2017

Free Radical Biology and Medicine 112 (2017) 350–359

Contents lists available at ScienceDirect

Free Radical Biology and Medicine

journal homepage: www.elsevier.com/locate/freeradbiomed

Bcl-x_L knockout attenuates mitochondrial respiration and causes oxidative stress that is compensated by pentose phosphate pathway activity

Annika Pfeiffer[a], Julia Schneider[a], Diones Bueno[a], Amalia Dolga[b], Timo-Daniel Voss[c], Jan Lewerenz[c], Verena Wüllner[a], Axel Methner[a,*]

[a] Department of Neurology, University Medical Center and Focus Program Translational Neuroscience (FTN) of the Johannes Gutenberg-University Mainz, Langenbeckstr. 1, 55131 Mainz, Germany
[b] Department of Molecular Pharmacology, University of Groningen, Antonius Deusinglaan 1, 9713 AV Groningen, The Netherlands
[c] Universitäts, und Rehabilitationskliniken Ulm, Oberer Eselsberg 45, 89081 Ulm, Germany

ARTICLE INFO

Keywords:
Bcl-xL
Mitochondria
Mitochondrial respiration
Oxidative stress
Pentose phosphate pathway

ABSTRACT

Bcl-x_L is an anti-apoptotic protein that localizes to the outer mitochondrial membrane and influences mitochondrial bioenergetics by controlling Ca^{2+} influx into mitochondria. Here, we analyzed the effect of mitochondrial Bcl-x_L on mitochondrial shape and function in knockout (KO), wild type and rescued mouse embryonic fibroblast cell lines. Mitochondria of KO cells were more fragmented, exhibited a reduced ATP concentration, and reduced oxidative phosphorylation (OXPHOS) suggesting an increased importance of ATP generation by other means. Under steady-state conditions, acidification of the growth medium as a readout for glycolysis was similar, but upon inhibition of ATP synthase with oligomycin, KO cells displayed an instant increase in glycolysis. In addition, forced energy production through OXPHOS by replacing glucose with galactose in the growth medium rendered KO cells more susceptible to mitochondrial toxins. KO cells had increased cellular reactive oxygen species and were more susceptible to oxidative stress, but had higher glutathione levels, which were however more rapidly consumed under conditions of oxidative stress. This coincided with an increased activity and protein abundance of the pentose phosphate pathway protein glucose-6-phosphate dehydrogenase, which generates NADPH necessary to regenerate reduced glutathione. KO cells were also less susceptible to pharmacological inhibition of the pentose phosphate pathway. We conclude that mitochondrial Bcl-x_L is involved in maintaining mitochondrial respiratory capacity. Its deficiency causes oxidative stress, which is associated with an increased glycolytic capacity and balanced by an increased activity of the pentose phosphate pathway.

1. Introduction

The yin and yang of life and death is regulated to a significant degree by members of the Bcl-2 (B-cell lymphoma protein 2) family, which regulate the execution of apoptosis, the cell death program essential for normal development and homeostasis of a multicellular organism (reviewed by [1]). The two most prominent anti-apoptotic family members, Bcl-2 and Bcl-x_L (Bcl-2-related protein, long isoform), share a common structure with four conserved Bcl-2 homology domains and a C-terminal membrane anchor, but differ in their subcellular localization. Bcl-2 distributes on several intracellular membranes, whereas Bcl-x_L is mainly targeted to the outer mitochondrial membrane (OMM) [2]. Both proteins interact with the inositol 1,4,5-triphosphate (InsP3) receptor (InsP3R) Ca^{2+} release channel at the endoplasmic reticulum (ER), although with different domains and with opposite effects. Whereas Bcl-2 reduces the InsP3R-mediated intracellular Ca^{2+} release [3–5], Bcl-x_L sensitizes InsP3Rs to low agonist concentrations, which stimulates Ca^{2+} oscillations and Ca^{2+} flux into the cytosol, thereby enhancing mitochondrial bioenergetics [6,7]. In mouse embryonic fibroblasts (MEFs) derived from *bcl-x* knockout (KO) animals,

Abbreviations: 2-DG, 2-Deoxy-D-glucose; ADP, adenosine diphosphate; Ama, antimycin A; ATP, adenosine triphosphate; c, cytochrome c; Bcl-x_L, B-cell lymphoma protein 2-related protein, long isoform; dig, digitonin; E, electron transfer system capacity state; ECAR, extracellular acidification rate; ER, endoplasmic reticulum; ETS, electron transfer system; FCCP, carbonyl cyanide 4-(trifluoromethoxy) phenylhydrazone; FCS, fetal calf serum; G, glutamate; GSH, reduced glutathione; GSSG, glutathione disulfide/oxidized glutathione ICC, immunocytochemistry; KO, knockout; L, leak state;; M, malate; NAD, nicotinamide adenine dinucleotide; OMM, outer mitochondrial membrane; Omy, oligomycin; OXPHOS, oxidative phosphorylation; P, OXPHOS capacity state; PPP, pentose phosphate pathway; R, routine state; Rot, rotenone; ROX, residual oxygen consumption; RT, room temperature; S, succinate; SUIT, substrate-uncoupler-inhibitor titration; PCP, phosphorylation-control protocol

* Correspondence to: Johannes Gutenberg University Medical Center Mainz, Department of Neurology, Langenbeckstr. 1, D-55131 Mainz, Germany.
E-mail address: axel.methner@gmail.com (A. Methner).

http://dx.doi.org/10.1016/j.freeradbiomed.2017.08.007
Received 10 March 2017; Received in revised form 1 August 2017; Accepted 8 August 2017
Available online 12 August 2017
0891-5849/

which also lack the pro-apoptotic alternative splice variant Bcl-x_s, only re-expression of mitochondrially targeted, but not ER-localized Bcl-x_L, restored protection against anti-apoptotic stimuli to levels observed in wildtype (WT) cells [8]. ER-targeted Bcl-x_L, in contrast, restored the ER Ca^{2+} homeostasis suggesting two independent functions of Bcl-x_L, depending on localization to the ER or the mitochondria [8].

Bcl-x_L also affects the constantly ongoing mitochondrial fusion and fission that keeps mitochondria healthy through the exchange of mitochondrial DNA, proteins and lipids between defective and functional mitochondria. These highly dynamic processes are important for mitochondrial bioenergetics and cellular survival (reviewed in [9]). In rat cortical neurons over-expressing Bcl-x_L, mitochondria are elongated, and in knockout neurons more fragmented [10]. Bcl-x_L influences mitochondrial dynamics by interacting with the mitochondrial fusion proteins mitofusin 1 (Mfn1) and 2 [11], as well as with the mitochondrial fission factor Drp-1 [12], by increasing their respective functions. It was postulated that Bcl-x_L promotes both mitochondrial fusion and fission dependent on the relative protein expression level of Bcl-x_L [13,14].

Bcl-x_L also affects mitochondrial function. Over-expression in hippocampal neurons caused an enhanced and more efficient energy metabolism, based on an increase in ATP production and decreased mitochondrial oxygen uptake, reflecting a more efficient coupling between ATP production and oxygen uptake [15]. Here, the proposed mechanism postulated an additional localization of Bcl-x_L in the inner mitochondrial membrane and a direct interaction with the β-subunit of the F_1F_o ATP synthase [15]. In addition, neurons deficient for *bcl-x* displayed large fluctuations in inner mitochondrial membrane potential, indicating increased total ion flux in and out of mitochondria and suggesting a role for Bcl-x_L in the reduction of futile ion flux across the inner mitochondrial membrane [16]. An alternative mechanism of how Bcl-x_L affects the mitochondrial function involves the interaction of Bcl-x_L with voltage-dependent anion channels (VDAC) at the OMM [17,18]. VDAC channels are responsible for the regulated crossing of metabolites and Ca^{2+} through the membrane and are of utmost importance for the correct functioning of mitochondria [19]. Recently, Huang et al. found a reduced mitochondrial Ca^{2+} uptake in the same Bcl-x-KO cells described above in response to agonist-induced ER Ca^{2+} release, which was restored by re-expression of mitochondrially targeted Bcl-x_L [20]. Interestingly, peptides based on the VDAC sequence that disrupted Bcl-x_L binding also reduced mitochondrial Ca^{2+} uptake in wild type (WT), but were without effect in Bcl-x-KO cells. The authors concluded that an interaction between Bcl-x_L and VDAC promotes matrix Ca^{2+} accumulation by increasing Ca^{2+} transfer across the OMM. As elevated mitochondrial matrix [Ca^{2+}] stimulates Krebs' cycle dehydrogenases and elevates mitochondrial [NADH] that is fed into the oxidative phosphorylation pathway [6], this should increase mitochondrial respiration. Therefore, we expected that Bcl-x_L deficiency influences mitochondrial respiratory activity and changes mitochondrial morphology.

Here, we performed an in-depth analysis of the effect of mitochondrial Bcl-x_L on mitochondrial shape and function in well-characterized Bcl-x-KO, WT and rescue MEF cell lines. We found that mitochondrial Bcl-x_L controls mitochondrial respiratory capacity and ATP production. Its deficiency leads to more fragmented mitochondria, an increase in glycolytic capacity and an increase in non-mitochondrial oxidative stress, which is compensated by increased activity of the pentose phosphate pathway.

2. Material and methods

2.1. Cell culture

The MEF cell lines WT, Bcl-x-KO and Bcl-x_L-ActA (kind gift of Carl White, Chicago, USA) [8] were cultured in DMEM high glucose (#E15-843, PAA, Pasching, Austria; #D6429, Sigma-Aldrich, Steinheim, Germany; or #41966029, Gibco, Paisley, United Kingdom) supplemented with 10% (v/v) fetal calf serum (FCS; Thermo Scientific, Rockford, IL, USA), 100 U/ml penicillin and 100 µg/ml streptomycin (Gibco) in a humidified incubator at 5% CO_2 and 95% air at 37 °C. Bcl-x_L-ActA MEFs stably over-express a Bcl-x_L where the C-terminal transmembrane sequence is replaced by the membrane-targeting sequence of the listerial protein ActA to target Bcl-x_L specifically to mitochondria [8]. These cells were grown in medium supplemented with 1.5 µg/ml blasticidin (#ant-bl-1, InvivoGen, Toulouse, France).

2.2. Immunoblotting

Denatured total cellular protein samples in RIPA buffer (#89900, Thermo Scientific) supplemented with 1x LDS (#NP007, Invitrogen) or Laemmli sample buffer (#1610747, BioRad) (95 °C, 5 min) were separated on SDS polyacrylamide gels (8–16% Precise Protein Gels (Thermo Scientific) or 4–15% Mini-PROTEAN® TGX Stain-Free™ gels (Bio-Rad Laboratories GmbH, München, Germany) and transferred onto a membrane (nitrocellulose or PVDF) using the iBlot Dry Blotting System (Invitrogen, Darmstadt, Germany) or Trans-Blot® Turbo™ Transfer System (Bio-Rad). Membranes were blocked with 3% (w/v) milk powder in PBS-T (1x PBS, 0.05% (v/v) Tween 20, blocking buffer) for 1 h at room temperature (RT). The membrane was incubated at 4 °C overnight with the primary antibodies anti-Bcl-$x_{S/L}$ (S-18) (1:100–1:200; #sc-634, Santa Cruz Biotechnology, Heidelberg, Germany), anti-G6PD (D5D2) (1:1000; #12263, Cell Signaling, Frankfurt, Germany), anti-actin (clone C4) (1:4000; #MAB1501, Merck Millipore, Darmstadt, Germany) in blocking buffer. For visualization, membranes were incubated with infrared fluorescence IRDye 680 and 800-conjugated anti-mouse/anti-rabbit IgG secondary antibodies (1:30,000; Licor, Königstein, Germany) in blocking buffer for 1 h at RT and detected with the Odyssey Infrared (Sa) Imaging System (Licor). The software ImageJ (http://imagej.nih.gov/ij/) was used to analyze the expression of proteins in relation to the control.

2.3. Immunocytochemistry

Cells transfected with pDsRed2-mito were seeded onto cover slips and fixed the next day with 4% Roti®-Histofix (15 min at RT) (#P087.4, Carl Roth, Karlsruhe, Germany), permeabilized and blocked with 1x ROTI-Immunoblock in PBS (#T144.1, Carl Roth) supplemented with 0.5% (w/v) n-octyl-β-D-glucopyranoside (Carl Roth; ICC blocking buffer) (60 min at RT). The primary antibody anti-Bcl-x_L (54H6) (#2764, Cell Signaling) was diluted 1:200 in the ICC blocking buffer and cover slips were incubated at 4 °C overnight. The fluorescein isothiocyanate (FITC)-conjugated secondary antibody was diluted in the same ICC blocking buffer and cells were incubated for 1 h at RT before cell nuclei were stained with 300 nM DAPI (5 min, RT). Cover slips were mounted with Dako Fluorescent Mounting Medium (#S3023, Dako, Glostrup, Denmark) onto microscope slides and fluorescence pictures were taken with the same settings from one optical section using a 63× oil immersion objective with the confocal microscope TCS SP5 from Leica (Leica Microsystems, Wetzlar, Germany).

2.4. Analysis of the mitochondrial morphology

Cells were transfected with mitochondrially targeted DsRed2, a red fluorescent protein, using the Attractene Transfection Reagent (#301005, Qiagen, Hilden, Germany) according to the manufacturer's instruction. One day after transfection, cells were seeded onto cover slips. The next day, cells were fixed with 4% Roti®-Histofix for 15 min at RT, permeabilized with 0.2% (v/v) Triton X-100 in PBS for 10 min and then cell nuclei were stained with 300 nM DAPI (5 min, RT). Cover slips were mounted onto microscope slides using Dako Fluorescence Mounting Medium. Cells were categorized by a blinded observer and representative pictures were taken with an Olympus BX51 fluorescence

microscope using a 60× oil immersion objective. In total, 200 cells per condition were analyzed and categorized.

2.5. Measurement of mitochondrial oxygen consumption

The mitochondrial oxygen consumption was analyzed with the high-resolution respirometer Oxygraph-2k (Oroboros Instruments, Innsbruck, Austria) using the DatLab Software 5.1. The oxygen concentration (nmol/ml) and the oxygen consumption expressed as oxygen flow per cells (pmol/(s*10^6 cells)) were recorded in 2 s intervals at a gain of 2. The oxygen consumption of cells was examined under continuous stirring at 750 rpm and 37 °C. A mitochondrial substrate-uncoupler-inhibitor titration (SUIT) protocol was carried out to study respiratory control and oxidative phosphorylation (OXPHOS) with digitonin-permeabilized cells. MEFs were analyzed in mitochondrial respiration medium MiR05 (0.5 mM EGTA, 3 mM $MgCl_2$ * $6H_2O$, 60 mM lactobionic acid (#153516, Sigma), 20 mM taurine (#T0625, Sigma), 10 mM KH_2PO_4, 20 mM HEPES, 110 mM D-sucrose (#4621.1, Roth), 1 g/l essentially fatty acid free BSA (PAA), pH 7.1) [21] at a density of 1.0–1.2 × 10^6 cells/ml. After measuring routine endogenous respiration, 2 mM malate (M; #M1000, Sigma) and 10 mM glutamate (G; G1626, Sigma) were added and cells were permeabilized with 13 µg digitonin (#D5628, Sigma) per 10^6 cells to record the leak state GM_N (no adenylates added, N). Respiration was stimulated by adding 1 mM ADP (A5285, Sigma-Aldrich) and the OXPHOS capacity state (P) GM_P depending on complex I-linked respiration was examined. 10 mM succinate (S; #S2378, Sigma) was added, which induced respiration with convergent electron input of complex I and II into the Q-junction and the respiratory state GMS_P was determined. 2 mM ADP were added to exclude a limitation by ADP and the intactness of the outer mitochondrial membrane was verified by adding 10 µM cytochrome c (c; #C7752; Sigma) (state $GMSc_P$). The ATP synthase was inhibited with 2 µg/ml oligomycin and the leak state GMS_L was measured. Titration of FCCP in 0.5 µM steps stimulated respiration and the ETS state GMS_E was determined. Inhibition of complex I by addition of 0.5 µM rotenone allowed the evaluation of the respiratory capacity on succinate alone in the ETS state $S(Rot)_E$; ROX was determined after adding 2.5 µM antimycin A. All experiments were performed under instrumental background correction and after daily calibration of the polarographic oxygen sensor. ROX was used to correct all measured respiratory states to allow the comparison of mitochondrial oxygen consumption.

2.6. Quantification of mitochondrial ATP levels

Relative mitochondrial ATP levels were determined with mitoBTeam, a BRET-based ATP biosensor targeted to mitochondria [22]. WT, Bcl-x-KO and Bcl-x_L-ActA MEF cells were seeded into 96-well plates at a density of 5000 cells/well and transfected 24 h later using TurboFectin reagent (OriGene). 2 days later, cells were incubated for 30 min in phenol red-free DMEM containing 10% FBS, and 30 µM NanoLuciferase (NLuc) inhibitor to avoid disturbance from BTeam released from dead cells. Afterwards, NLuc substrate was added to the medium and the plate incubated for 20 min. Luminescence emissions from the cells were measured at 37 °C at 520/60 nm (Yellow Fluorescent Protein (YFP) emission) and at 430/70 nm (NLuc emission). Data are expressed as YFP/NLuc emissions ratio.

2.7. Cell viability assays

Cells were seeded at a density of 3000–5000 cells per well into 96-well plates as indicated. The next day, the pentose phosphate pathway inhibitor 6-aminonicotinamide (6-AN), glutamate, or the complex III inhibitor antimycin A and the ATP synthase inhibitor oligomycin were added in the indicated concentrations. Regular growth medium was replaced by DMEM without glucose supplemented with 25 mM galactose, 10% (v/v) FCS, 100 U/ml penicillin, 100 µg/ml streptomycin and 1 mM sodium pyruvate. 24 h later, cell viability was determined using the CellTiter Blue reagent (CTB; #G8081, Promega, Madison, WI, USA) and the fluorescent signal was recorded at 562 nm excitation/590 nm emission using the Infinite M200 Pro microplate reader (Tecan, Männedorf, Switzerland) after incubation under standard growth conditions for 3 h.

2.8. Analysis of the acidification rate using the Seahorse

Extracellular acidification rate (ECAR) measurements were assessed using an XF96 Extracellular Flux Analyzer (Seahorse Bioscience, North Billerica, MA). MEF cells were seeded in XF 96-well cell culture microplates (Seahorse Bioscience) at a density of 10,000 cells per well in standard culture medium and incubated at 37 °C and 5% CO_2 for 24 h. Before starting the measurements, the growth medium was washed and replaced with 180 µl of assay medium (DMEM supplemented with 2 mM glutamine, 1 mM pyruvate, pH 7.35) and cells were incubated at 37 °C for at least 60 min. Three baseline measurements were recorded before the addition of compounds. Glucose (25 mM) was injected in Port A (20 µl). The ATP synthase-inhibitor oligomycin was injected in Port B (22.5 µl) at a final concentration of 1 µM to measure ECAR in the absence of oxidative phosphorylation. The glycolysis blocker, 2-deoxy-D-glucose (2-DG) was subsequently injected in Port C (25 µl) at a concentration of 50 mM. Three measurements were performed after the addition of each compound by a 4-min mix cycle used to oxygenate the medium and a 3-min measurement cycle to assess glycolysis.

2.9. Enzymatic measurements of total cellular glutathione and glucose-6-phosphate dehydrogenase (G6PD)

Total cellular glutathione (GSH and GSSG) content was analyzed using an enzymatic assay. One day after plating 200,000 cells per well in 6-well plates, cells were treated with 10 mM glutamate for the indicated time. Cells were washed twice with ice-cold PBS before they were resuspended in 200 µl PBS and the cell suspension transferred into 100 µl of 10% (w/v) sulfosalicylic acid (#S7422, Sigma). After vortexing, the sample was incubated on ice for 10 min, centrifuged (10 min, 16,000*g* at 4 °C) and neutralized by transferring the supernatant into 24 µl of 50% (v/v) triethanolamine in H_2O (#90278, Sigma). In order to normalize the quantified total cellular glutathione content in the end, the pellet was solubilized in 100 µl of 0.2 N NaOH at 37 °C overnight and the protein concentration was quantified using a BC Assay Protein Quantitation Kit (#UP40840A, Interchim, Montlucon, France). The total cellular glutathione was quantified by diluting the sample in GSH Assay Buffer (100 mM Na_2PO_4, 1 mM EDTA, pH 7.5) supplemented with 0.8 mM NADPH (#N1630, Sigma), 0.6 mM 5,5′-dithiobis-(2-nitrobenzoic-acid) (DTNB; #D8130, Sigma) and 1 U/ml glutathione reductase (#G3664, Sigma). The formation of TNB was measured kinetically at 390 nm using the GENios Pro microplate reader (Tecan) in parallel to a standard with known glutathione concentration. G6PD activity was measured enzymatically as described previously [23,24].

2.10. Cell proliferation assay

In order to examine the cell proliferation of the MEF cell lines, 6250 cells per well were plated into a 24-well plate and left to adhere for 3–4 h. Cell growth was analyzed on day 0, 1 and 3 by replacing the growth medium with growth medium supplemented with CTB reagent. After incubation for 3 h under general growth conditions, 100 µl samples (three per well) were transferred to a 96-well plate and the fluorescent signal (562/590 nm excitation/emission) was measured using the Infinite M200 Pro microplate reader. The rest of the CTB-medium mix was removed and replaced by fresh growth medium to let the cells proliferate under standard growth conditions. In order to quantify the cell number, a standard curve of each cell line was prepared by plating

different cell numbers into a 24-well plate. Cells were left to adhere for 3–4 h before the corresponding fluorescent signal was determined using the CTB reagent.

2.11. Measurement of mitochondrial superoxide and cellular ROS levels

10,000 cells per well in 200 µl medium were plated in 8 well µ-slides ibiTreat (#80826, ibidi, Martinsried, Germany). 24 h later, MitoSox (#M36008, ThermoFisher) respectively CellRox (#C10443, Life Technologies) was added at a final concentration of 5 µM in Hank´s Buffered Salt Solution/Ca^{2+}/Mg^{2+} according to the manufacturer's protocol. Cells were incubated for 20 respectively 30 min at 37 °C and washed three times with warm HBSS. Confocal images were taken with a Leica TCS SP5 II microscope at 1024 × 1024 pixels. Images were captured using 63× oil immersion objective lens. MitoSox and CellRox were excited by laser at the given wavelength.

2.12. Statistical analysis

Data are presented as mean ± standard deviation (S.D.) or as Tukey plots. Statistical significance was assessed by the one-way Analysis of Variance (ANOVA) followed by the Tukey's multiple comparison test, the two-way ANOVA followed by the Bonferroni's post hoc test or the non-parametric Kruskal-Wallis ANOVA test followed by Dunn's multiple comparison test; a p-value less than 0.05 was considered statistically significant.

3. Results

3.1. Increased mitochondrial fragmentation in Bcl-x knockout cells

We obtained the mouse embryonic fibroblast cell lines previously described and studied by Eno [8] and Huang et al. [20] and first verified the lack of *bcl-x* expression in Bcl-x-KO cells by immunoblotting. KO cells indeed lacked Bcl-x_L, while the rescue cells Bcl-x_L-ActA expressed more Bcl-x_L than WT cells (Fig. 1). Bcl-x_L-ActA MEFs stably over-express Bcl-x_L specifically targeted to the outer mitochondrial membrane and were generated by replacing the original C-terminal transmembrane sequence with the membrane-targeting sequence of the listerial protein ActA [8]. The pro-apoptotic alternative splice variant Bcl-x_s was undetectable in all cell lines in line with previous observations [8]. Bcl-x_L also co-localized with transiently transfected mitochondrially targeted DsRed2 (mtDsRed), a red fluorescent protein, as expected (Fig. 2A) and the protein expression levels in all three cell lines reflected the abundance observed by immunoblotting (compare Figs. 1 and 2A). We then investigated the effect of Bcl-x_L on the mitochondrial shape by transiently expressing mtDsRed and categorizing mtDsRed-positive mitochondria as tubular, mixed, vesicular or fragmented (see exemplary pictures Fig. 2B). WT cells expressing endogenous Bcl-x_L protein had mainly tubular mitochondria, whereas Bcl-x-KO mitochondria were rather vesicular and fragmented (Fig. 2B). The re-expression of Bcl-x_L at mitochondria in Bcl-x_L-ActA cells changed the mitochondrial morphology towards WT cells, but a mixed morphology was still more abundant in these cells. We concluded that Bcl-x_L deficiency leads to a more fragmented mitochondrial shape and can be restored in part by re-expression of mitochondrial Bcl-x_L. Thus, mitochondrial Bcl-x_L affects mitochondrial dynamics and shifts mitochondrial morphology towards a more elongated phenotype.

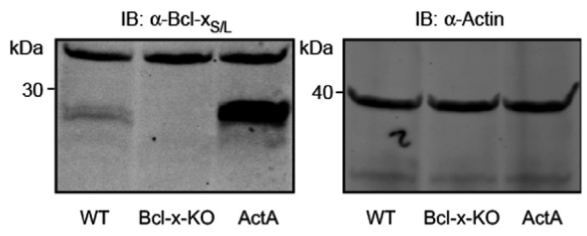

Fig. 1. Bcl-x knockout and mitochondrial rescue. Immunoblot demonstrating lack of Bcl-x_L in knockout cells (Bcl-x-KO) and Bcl-x_L expression in wild type (WT) and Bcl-x_L-ActA (ActA) cells. The blot was probed with an antibody directed against Bcl-$x_{S/L}$; β-Actin served as loading control, size is indicated.

3.2. Reduced mitochondrial respiratory capacity in Bcl-x-knockout cells

We next analyzed the mitochondrial respiratory activity of WT, Bcl-x-KO and Bcl-x_L-ActA cells by high-resolution respirometry to determine whether Bcl-x_L influences mitochondrial respiration. We studied the respiratory control and oxidative phosphorylation (OXPHOS) of these cell lines in a mitochondrial substrate-uncoupler-inhibitor titration (SUIT) protocol with digitonin-permeabilized cells in mitochondrial respiration medium. In this experiment the routine endogenous respiration, which depends on intracellular metabolites before permeabilization of the cells, was similar in all three lines (Fig. 3A), consistent with results obtained using non-permeabilized cells (not shown). After permeabilization, both measured leak respiratory states (state GM_N without added adenylates after addition of glutamate + malate, and the leak respiration state GMS_L directly after inhibition of the ATP synthase with oligomycin) were also comparable (Fig. 3A).

The OXPHOS state GM_P with glutamate/malate-supported respiration through complex I was in trend reduced in the Bcl-x-KO cells (oxygen flow per cells: 88.94 ± 19.6 pmol/(s*10^6)) compared to WT (99.27 ± 22.0 pmol/(s*10^6)) and Bcl-x_L-ActA cells (109.02 ± 17.2 pmol/(s*10^6)). Importantly, after addition of the substrate succinate the OXPHOS state GMS_P with convergent complex I and II electron input into the respiratory system was significantly reduced in Bcl-x-KO (106.80 ± 24.1 pmol/(s*10^6)) cells, but not in WT (127.75 ± 32.4 pmol/(s*10^6)) or Bcl-x_L-ActA (134.81 ± 19.5 pmol/(s*10^6)) cells. In line with this, the electron transfer system (ETS) capacity GMS_E with convergent complex I and II electron input was significantly lower in MEFs lacking Bcl-x_L (140.13 ± 33.7 pmol/(s*10^6)) compared to WT cells (159.34 ± 34 pmol/(s*10^6)). Moreover, re-expression of mitochondrially targeted Bcl-x_L in Bcl-x-KO MEFs significantly increased GMS_E to 166.13 ± 25.2 pmol/(s*10^6) in Bcl-x_L-ActA cells. Re-expression of mitochondrially targeted Bcl-x_L thus rescues the effect of Bcl-x_L deficiency and increases both respiratory states in Bcl-x_L-ActA cells up to comparable levels in WT cells. In contrast, the ETS capacity $S(Rot)_E$ after inhibition of complex I, which depends on succinate-supported electron input via complex II, was similar in all cell lines. This suggests a low capacity of succinate-supported respiration. The lower oxygen flow per cells at the OXPHOS capacity state (GMS_P) compared to the maximum ETS capacity state (GMS_E) indicates a restriction of respiration by the phosphorylation system. Thus, all cell lines had clear excess in their ETS capacity. The restriction by the phosphorylation system also limited the stimulation of respiration after addition of succinate suggesting that the phosphorylation system retains control over respiratory flux. The addition of cytochrome c in this experimental set-up proved the intactness of the OMM because cytochrome c addition only facilitated an increase of less than 15% in the oxygen flow per cells (state $GMSc_P$) and only these experiments were considered in the analysis.

The OXPHOS control ratio P/E (GMS_P/GMS_E) – this is the part of the maximum ETS capacity used for OXPHOS – was significantly lower in MEFs lacking Bcl-x_L compared to WT MEFs and again, expression of Bcl-x_L-ActA increased the P/E ratio of Bcl-x-KO MEFs to WT levels (Fig. 3B). This reduced P/E ratio in Bcl-x-KO cells indicates that the control of the phosphorylation system is stronger in the absence of Bcl-x_L. The leak control ratio L/E (GMS_L/GMS_E), in contrast, was comparable in all cell lines. In conclusion, these results suggest that the presence of Bcl-x_L at mitochondria influences mitochondrial

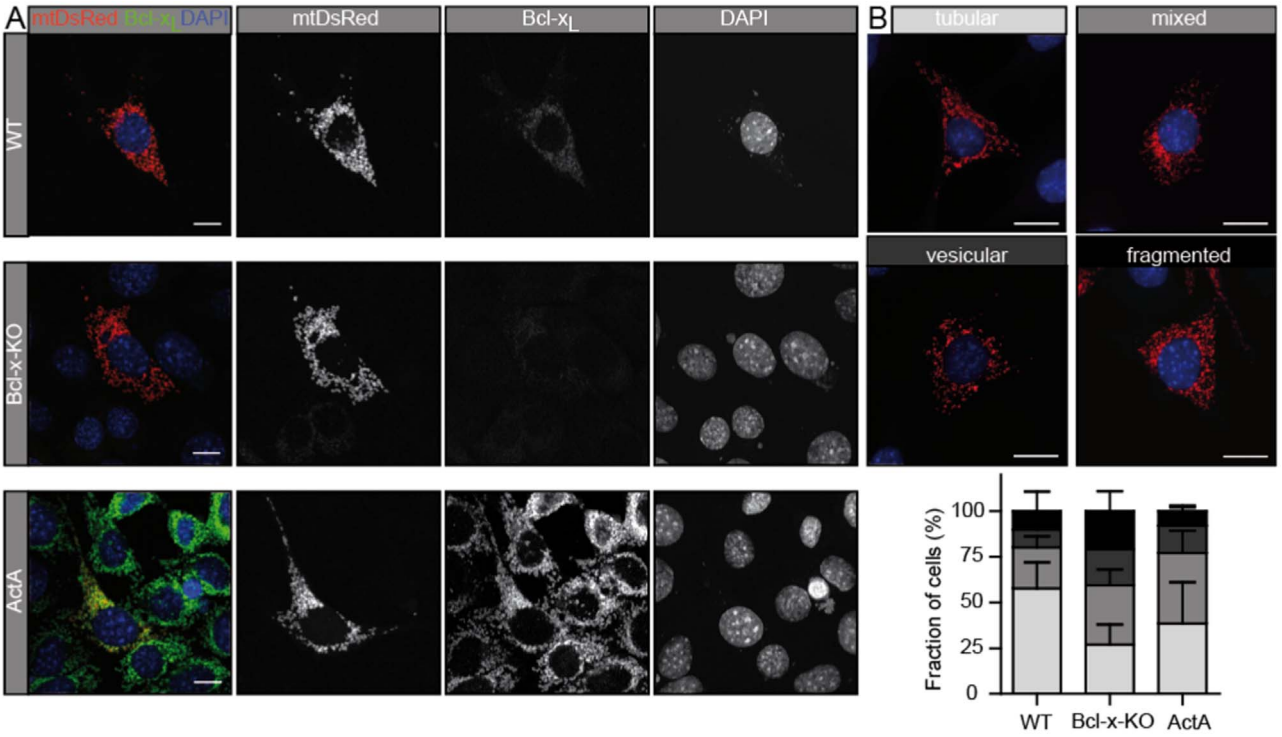

Fig. 2. Increased mitochondrial fragmentation in Bcl-x-KO cells. (A) Bcl-x_L co-localizes with mitochondria. Cells were transiently transfected with mitochondrially targeted DsRed2 (mtDsRed, red), a red fluorescent protein, and stained with an antibody directed against Bcl-x_L (green). Scale bar represents 10 μm. (B) Increased mitochondrial fragmentation in Bcl-x-KO cells. Cells were transiently transfected with mtDsRed (red) and analyzed by fluorescence microscopy by a blinded observer. The mitochondrial morphology was categorized as tubular, mixed, vesicular or fragmented as indicated. Scale bar represents 20 μm. (C) Quantification of morphology depicted in B. The data are presented as mean ± S.D. of three independent experiments with n = 200 cells analyzed per experiment. (For interpretation of the references to color in this figure legend, the reader is referred to the web version of this article).

respiration, and deficiency of Bcl-x_L reduces the OXPHOS and ETS capacity state with convergent complex I and II electron input. In line with this, mitochondrial ATP production measured with mitochondrially targeted BTeam, an ATP sensor [22], was significantly reduced in KO cells, while re-expression of mitochondrially targeted Bcl-x_L increased the mitochondrial ATP content in Bcl-x_L-ActA cells to the levels observed in WT cells (Fig. 3C).

3.3. Inhibition of mitochondrial respiration increases extracellular acidification in Bcl-x-KO cells

Because of the reduced OXPHOS and ETS capacity of KO cells, we considered that these cells are more dependent on energy production by glycolysis and analyzed the extracellular acidification rate (ECAR) using a Seahorse apparatus. This surprisingly demonstrated similar acidification of the extracellular growth medium in the presence of glucose. Only upon addition of oligomycin, which inhibits mitochondrial ATP synthase, KO cells did react with an instant surge in acidification of the growth medium suggesting an immediate demand in energy production met by glycolysis (Fig. 4A).

To complement these data, we then studied the susceptibility of KO cells to mitochondrial toxins under normal conditions and under conditions where glycolysis is less favored by replacing glucose with galactose in the culture medium. Galactose modulates the energy metabolism and forces the cells to sustain most of their energy demand by OXPHOS since under these conditions the cells use glutamine mainly as a source to produce ATP in mitochondria [25]. We blocked OXPHOS with the mitochondrial toxins antimycin A (Fig. 4B) to inhibit complex III [26] or oligomycin (Fig. 4C) to inhibit ATP synthase [27]. Under normal conditions, all cell lines were similarly susceptible to the mitochondrial toxins. KO cells were, however, more vulnerable under conditions of perturbed glycolytic energy production (Fig. 4B and C). We interpreted these data as a further indication that Bcl-x-KO cells have a higher energy demand per se, which is normally met even by the compromised mitochondria and deteriorates only when glycolysis and OXPHOS are disturbed.

3.4. Absence of Bcl-x_L causes non-mitochondrial oxidative stress that is compensated by increased glutathione synthesis

So what causes this increased energy demand in the absence of Bcl-x_L? A previous study demonstrated an increased susceptibility of Bcl-x-KO MEFs not only to apoptotic stimuli, but also to H_2O_2-induced oxidative stress [8]. We therefore considered that Bcl-x-KO cells might suffer from increased on-going oxidative stress and spend energy for continuous antioxidant defense. In line with this, we found that Bcl-x-KO cells were more susceptible to oxidative stress (Fig. 5A). We elicited endogenous oxidative stress with glutamate; glutamate inhibits the concentration-driven glutamate/cystine-antiporter xCT, leading to deprivation of intracellular cysteine, the reduced form of cystine and the limiting amino acid for the synthesis of the major cellular antioxidant glutathione (reviewed in [28]). Cells therefore succumb to glutamate because of glutathione depletion and a reduced defense against the continuous production of reactive oxygen species (ROS) in living cells. In these experiments, we also noticed that Bcl-x-KO had a higher proliferation rate which we reproduced in independent experiments (Fig. 5B). We then quantified cellular ROS with CellROX and mitochondrial superoxide with MitoSox under steady-state conditions to elucidate the source of the suspected differences in ROS levels and found increased cellular ROS, but decreased mitochondrial superoxide levels in Bcl-x-KO cells (Fig. 5C). Interestingly, we also observed increased GSH levels in KO cells (Fig. 5D), which were however rapidly consumed after inhibition of glutathione synthesis by glutamate (Fig. 5D). We concluded that Bcl-x-KO cells suffer from ongoing oxidative stress, which is compensated under steady-state conditions by increased glutathione synthesis or recycling.

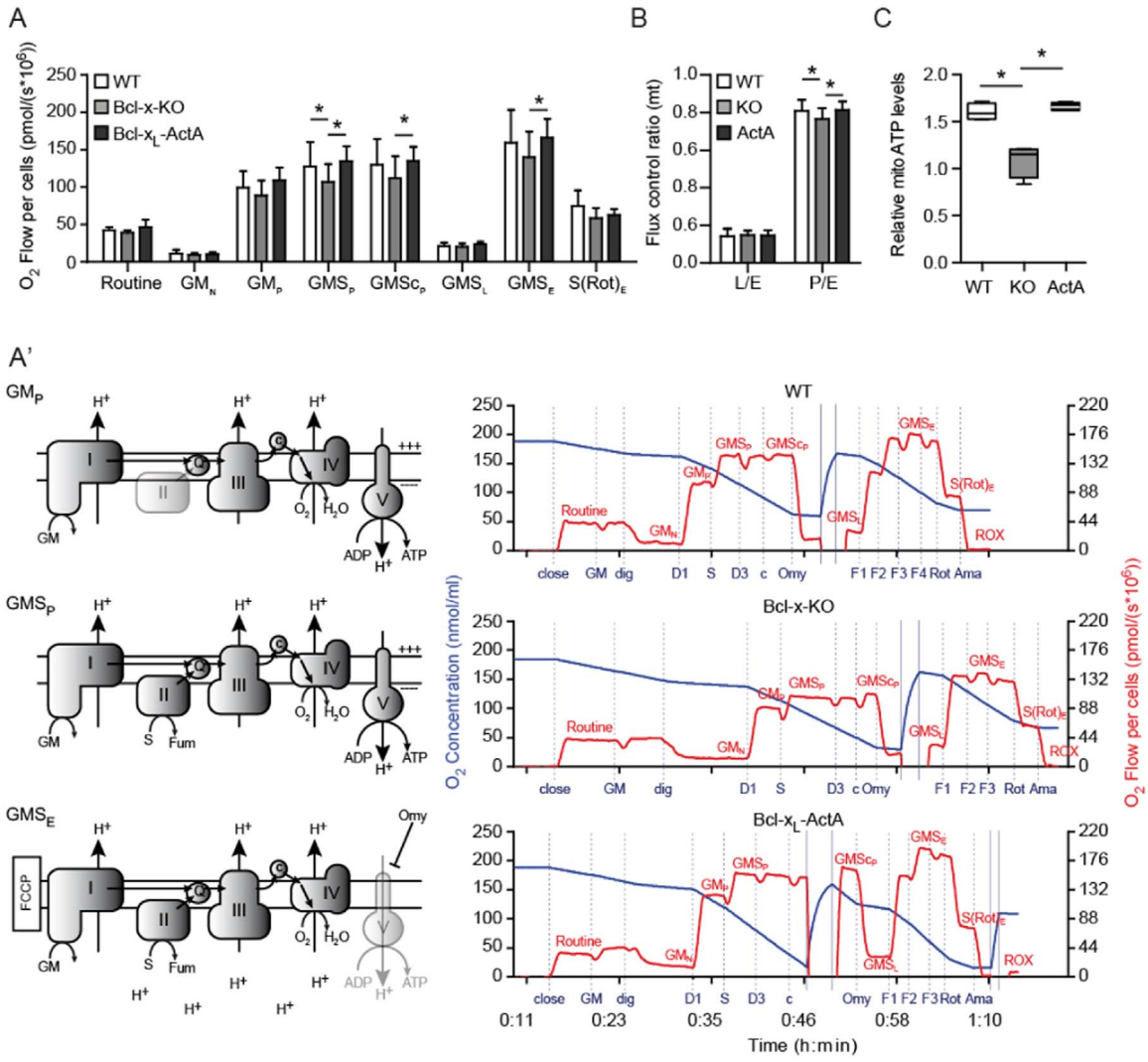

Fig. 3. Reduced mitochondrial respiratory capacity in Bcl-x-KO cells. (A) The OXPHOS capacity of mitochondrial respiration was studied by high-resolution respirometry of digitonin-permeabilized cells using the SUIT protocol. (A') Representative measurements of WT, Bcl-x-KO and Bcl-x$_L$-ActA cells indicating the oxygen concentration with blue traces (left axis) and the oxygen flow per cells with red traces (right axis) plotted against time. The additions of glutamate + malate (GM), digitonin (dig), ADP-Mg^{2+} (D including final concentrations: D1, 1 mM; D3, 3 mM), succinate (S), cytochrome c (c), oligomycin (Omy), FCCP (F including step number), rotenone (Rot) and finally antimycin A (Ama) are marked with vertical dashed lines. Vertical solid lines indicate re-oxygenation of the chambers including opening and closing. The measured and analyzed respiratory states are labeled in red, which were corrected for non-mitochondrial residual oxygen consumption (ROX; (A)). The illustrations on the left represent the OXPHOS capacity states GM$_P$ and GMS$_P$ as well as the electron transfer system capacity GMS$_E$. (A) Bcl-x-KO cells have a reduced OXPHOS capacity (GMS$_P$) as well as a reduced electron transfer system (ETS) capacity (GMS$_E$) with a convergent complex I and II input in the respiratory system. The over-expression of mitochondrially targeted Bcl-x$_L$ increases GMS$_P$ and GMS$_E$ up to levels comparable with WT cells and hence, rescues the effect of Bcl-x$_L$ deficiency. (B) Calculation of the mitochondrial (mt) leak control ratio (L/E = GMS$_L$/GMS$_E$) and the OXPHOS control ratio (P/E = GMS$_P$/GMS$_E$) indicated a significant decrease in the OXPHOS control ratio of Bcl-x-KO compared to WT and Bcl-x$_L$-ActA cells. Oxygraph O2k data presented in mean ± S.D. were collected in eight separate experiments, which were performed in duplicates (A/B). (C) Measurement of mitochondrial ATP levels using BTeam. Bcl-x-KO cells have a significantly reduced ATP content compared with WT and Bcl-x$_L$-ActA cells. Data were collected from n = 4 independent experiments done in triplicates and are presented as a Tukey box plot. An asterisk represents statistical significance ($p < 0.05$) as analyzed by two-way ANOVA and Bonferroni post-hoc tests (A and B) or the non-parametric Kruskal-Wallis test followed by Dunn's multiple comparison test (C). (For interpretation of the references to color in this figure legend, the reader is referred to the web version of this article).

3.5. Bxl-xL deficiency redirects glucose metabolism into the pentose phosphate pathway

Based on the observations that Bcl-x-KO cells have increased levels of glutathione and an increased proliferation rate, we hypothesized that KO cells increase glucose consumption in the pentose phosphate pathway (PPP; also known as the hexose monophosphate shunt). The PPP elevates NADPH production which is important for the recovery of oxidized glutathione and has a prominent anabolic function by generating phosphopentoses and ribonucleotides [29]. Increased PPP activity could thus explain both increased GSH and increased proliferation. Immunoblotting indeed demonstrated that the enzyme glucose-6-phosphate dehydrogenase (G6PD), often referred as the rate-limiting enzyme of this pathway located in the oxidative branch [30], was more abundant in KO and, to a lesser extent, also in Bcl-x$_L$-ActA cells (Fig. 6A). Furthermore, G6PD activity was significantly upregulated in KO cells and reduced under re-expression of mitochondrial localized Bcl-x$_L$ (Fig. 6B).

We therefore tried to clarify whether inhibition of the PPP with 6-aminonicotinamide (6-AN) [31] would differently affect viability in Bcl-x-KO and WT cells. 6-AN alone had no effect on viability (not shown), but was slightly toxic when combined with mild additional oxidative stress elicited with 2.5 mM glutamate. Under these conditions, Bcl-x-KO cells were protected against higher concentrations of 6-AN in line with the increased activity of the PPP in KO cells (Fig. 6C).

Based on these observations, we conclude that Bcl-x-KO cells suffer from continuous mild oxidative stress, which is compensated under non-stressed conditions by increased shuttling of glucose through the

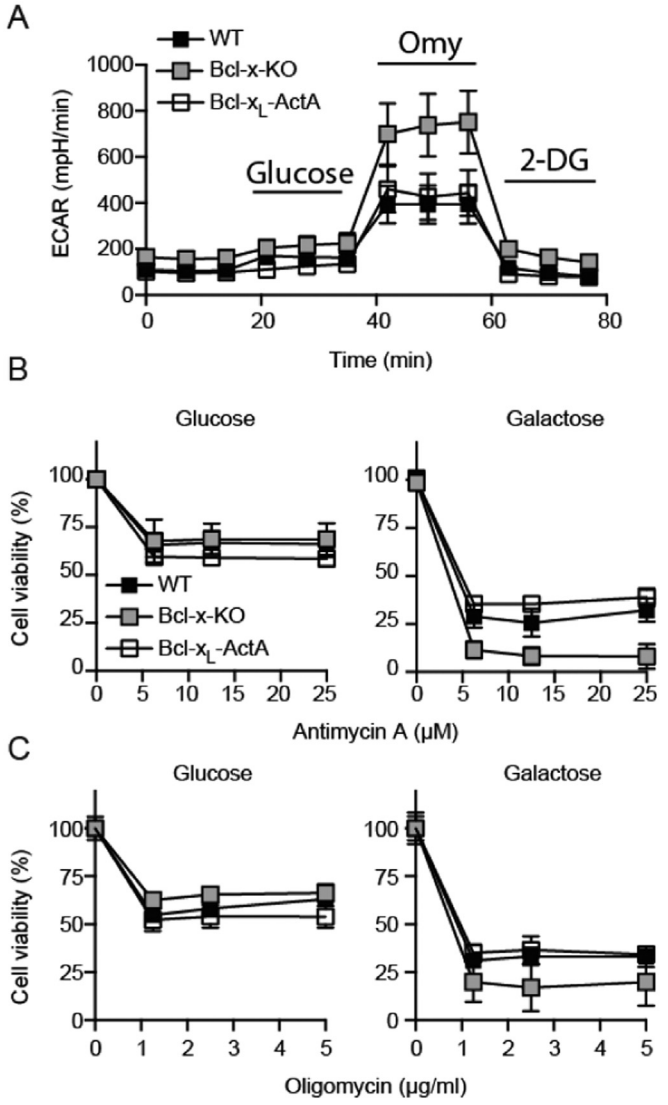

Fig. 4. Bcl-x-KO cells are susceptible to inhibition of OXPHOS and demonstrate a higher ATP demand. (A) Extracellular acidification rate (depicted as ECAR) was analyzed using a Seahorse Bioscience XF96 Flux Analyzer system. Before the measurements, cells were deprived of glucose for at least one hour. Following the background measurements, glucose (25 mM) was injected in Port A, followed by injection of Oligomycin (Omy; 1 µM) in Port B and 2-Deoxy-D-glucose (2-DG; 500 mM) in Port C. Data are expressed as mean ± S.D. (n ≥ 3). (B/C) Modulating energy metabolism by replacing glucose with galactose in the growth medium to prevent energy production in glycolysis and to force cells to sustain their energy demand by OXPHOS increases the susceptibility to inhibitors of mitochondrial respiration in Bcl-x-KO cells. 4000 cells plated into 96-well plates were treated with the indicated concentration of (B) the complex III-inhibitor antimycin A or (C) the ATP synthase-inhibitor oligomycin in medium containing either 25 mM glucose or 25 mM galactose. Viability was determined 24 h later using the CellTiter Blue reagent and normalized. Each experiment was performed three to four times in triplicates. The cell viability in percent as mean ± S.D. is plotted against antimycin A or oligomycin concentration as indicated.

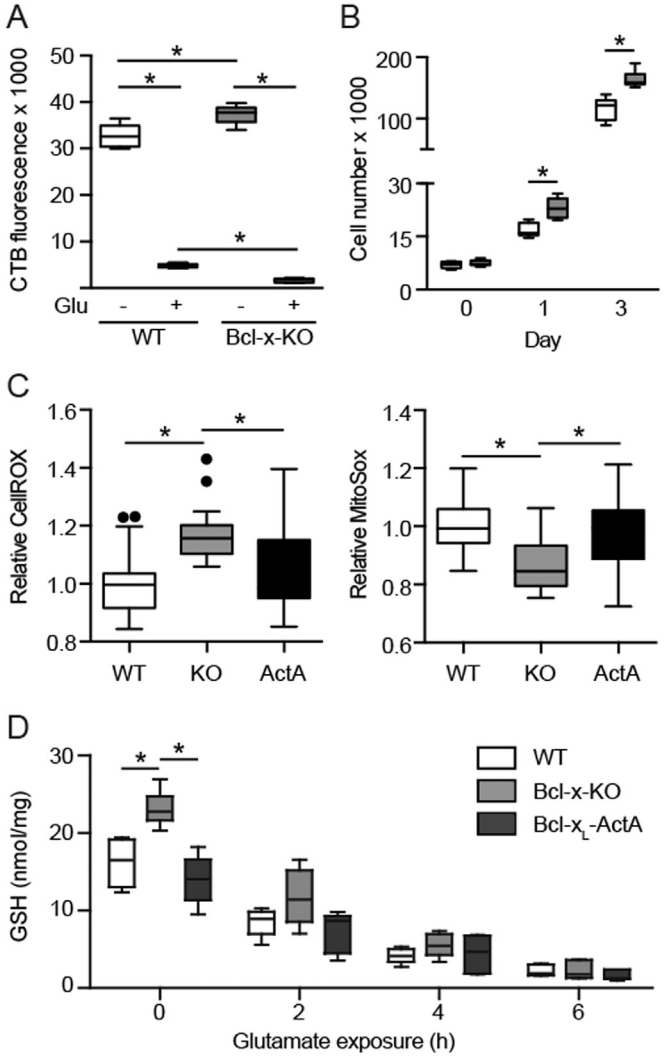

Fig. 5. Absence of Bcl-x$_L$ causes non-mitochondrial oxidative stress that is compensated by increased glutathione synthesis (A) Bcl-x-KO cells are more susceptible to endogenous oxidative stress caused by glutamate. 5000 WT and KO cells were seeded into 96-well plates and treated with 7.5 mM glutamate 24 h later. Cell viability was quantified by the CellTiter blue (CTB) assay again 24 h later. (B) Bcl-x-KO cells have a higher proliferation rate. 6250 cells were seeded into 24-well plates and analyzed on day 0, 1 and 3 by CTB assays. Data were collected from n = 3 independent experiments done in triplicates and are presented as a Tukey box plots. (C) Bcl-x-KO cells have higher cellular ROS, but decreased mitochondrial superoxide levels measured with CellROX and MitoSOX, two live-cell stains. Data were collected from n = 23–28 cells from three independent experiments and are presented as a Tukey box plots. (D) Increased total cellular glutathione content in Bcl-x-KO cells in steady state. Total cellular glutathione (GSH and GSSG) content (depicted as GSH) was measured enzymatically and normalized to the total protein content. Cells were treated for the indicted time with 10 mM glutamate. n = 3 independent experiments done in duplets. All data are presented as Tukey box plots and statistical significance assessed by the non-parametric Kruskal-Wallis ANOVA test followed by Dunn's multiple comparison test. Asterisks indicate $p < 0.05$.

PPP and consecutive increased GSH recycling (Fig. 7).

4. Discussion

Bcl-x$_L$ is best known for its role in apoptosis, but our work indicates that it also has an additional physiological role in mitochondrial shape and function in line with previous work. We found that Bcl-x$_L$-deficient cells have more fragmented mitochondria, a reduced mitochondrial respiratory capacity and a reduced mitochondrial ATP content. Our results also demonstrate that Bcl-x KO causes increased oxidative stress, which is compensated under non-stressed conditions by an enhanced activity of the pentose phosphate pathway. Loss of Bcl-x$_L$ therefore leads to a quite remarkable remodeling of cellular metabolism. The source of the increased ROS observed in Bcl-x-KO cells is probably not the malfunctioning mitochondria as we measured rather reduced mitochondrial superoxide levels in KO cells. Mitochondrial dysfunction can however also lead to the generation of other reactive oxygen species besides superoxide (reviewed in [32]). Also increased glucose uptake, which we have not directly measured, increases intracellular ROS production [33,34].

One limitation of our study is of course the use of immortalized cell lines, but increased mitochondrial fragmentation was previously also

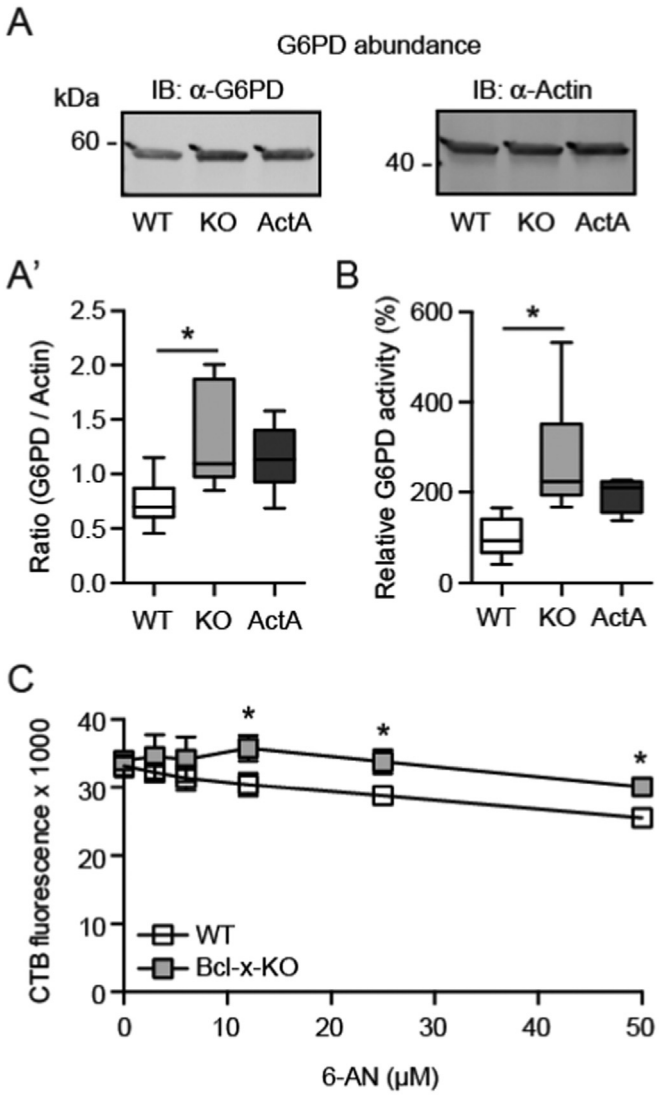

Fig. 6. Bxl-xL deficiency redirects glucose metabolism into the pentose phosphate pathway. (A/A') Increased expression of Glucose-6-phosphate dehydrogenase (G6PD) in Bcl-x-KO cells shown by immunoblotting. β-Actin served as loading control. Size is indicated, n = 9 blots. (B) Increased activity of G6PD in Bcl-x-KO cells quantified enzymatically, n = 3 independent experiments done in duplets. All data are presented as Tukey box plots and statistical significance assessed by the non-parametric Kruskal-Wallis ANOVA test followed by Dunn's multiple comparison test. Asterisks indicate $p < 0.05$.

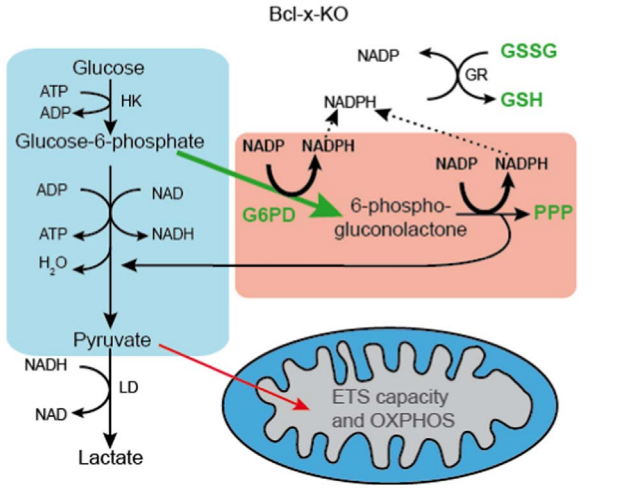

Fig. 7. Diagram depicting the observed changes in Bcl-x-KO cells. Bcl-x-KO cells showed a decrease in their OXPHOS and ETS capacity with a convergent complex I and II electron input, an increase in G6PD protein expression and activity and an enhancement in total cellular glutathione content. Thus, Bcl-x_L deficiency causes a reduction in mitochondrial respiratory capacity and an increase in pentose phosphate pathway activity (abbreviations: GR, glutathione reductase; HK, Hexokinase; LD, Lactate dehydrogenase; NAD, NAD+; NADP, NADP+).

observed in a conditional knockout of *bcl-x* in mouse cortical neurons [10]. Apparently, Bcl-x_L interacts with the mitofusins responsible for mitochondrial fusion [11,13] and the mitochondrial fission factor Drp-1 [12]. It was proposed that Bcl-x_L over-expression increases both fission and fusion [10]. Berman and colleagues claimed that the elongated mitochondrial morphology observed by Bcl-x_L over-expression cannot be explained by enhanced mitochondrial fusion and fission rates, but is rather a consequence of increasing mitochondrial biomass. However, the cells investigated here previously displayed no difference in their mitochondrial biomass [20]; we did not re-investigate this. Extensive mitochondrial fragmentation also occurs during apoptosis before the activation of caspases [35]. Although these Bcl-x-KO cells are more susceptible to apoptotic cell death [8], we do not consider the increased number of fragmented mitochondria as an indication for ongoing apoptosis as we observed no difference in cell viability under general growth conditions. Bcl-x-KO cells even had an increased proliferation rate compared to WT and Bcl-x_L-ActA cells. This increased proliferation rate can be explained by the increased activity of the anabolic PPP in KO cells, which generates 5-carbon sugars, so called pentoses, and ribose 5-phosphate, a precursor for the synthesis of nucleotides [29]. We previously also observed an increased activity of the PPP in a neuronal cell line resistant to oxidative stress [24], and others found an increased activity of the PPP in cell lines resistant to amyloid beta toxicity, which contributes to the detrimental effects of Alzheimer's disease [23]. We therefore hypothesize that the main reason for the increased activity of the PPP in Bcl-x-KO cells is most probably its involvement in the defense against oxidative stress. The PPP recycles GSH from its oxidized form GSSG [36] by generating the reducing agent NADPH.

Alavian et al. previously reported that over-expression of Bcl-x_L in hippocampal neurons increased ATP production and decreased mitochondrial oxygen uptake, whereas Bcl-x_L deficiency reduced ATP synthesis [15], which we could reproduce for mitochondrial ATP content. Interestingly, these authors found Bcl-x_L not only in the OMM, but also in the inner mitochondrial membrane or the matrix where it directly interacts with the β-subunit of the F_1F_o ATP synthase [15]. The Bcl-x_L used in our study, however, contains the membrane targeting sequence of the listerial protein ActA, which targets it to the OMM, where it also co-localizes with the OMM protein Tom20 [8]. This would make an interaction with the β-subunit of the ATP synthase that looms into the matrix improbable. Also, Bcl-x_L interacts with VDAC1 and 3 in the OMM and re-expression of the OMM-localized Bcl-x_L-ActA restores mitochondrial Ca^{2+} uptake in the Bcl-x knockout background [20], which also makes an interaction with the ATP synthase in the mitochondrial matrix unlikely. We therefore conclude that at least in Bcl-x_L-ActA cells the re-stored OXPHOS and ETS capacity is most probably not a result of such an interaction.

In our hands, mitochondrial oxygen consumption was similar in intact Bcl-x-KO, WT and Bcl-x_L-ActA cells, which is in line with the evidence suggesting that these cells have a comparable mitochondrial membrane potential [20]. We only observed a reduced OXPHOS and ETS capacity with convergent complex I and II electron input in permeabilized KO cells and hypothesized that this can be explained by changes in metabolite availability to the mitochondria. Bcl-x_L interacts with VDAC at the OMM [17,18,20,37–39]. VDAC regulates the flux of ions across the OMM and is important for the movement of metabolites like succinate, citrate, phosphocreatine and phosphate as well as for ATP/ADP exchange [40,41]. Efficient mitochondrial ATP/ADP exchange is required for coupled respiration. Growth factor withdrawal

from growth factor-dependent cells results in disruption of metabolism by defective ADP and ATP exchange across the mitochondrial membranes, which can be prevented by Bcl-x_L [41,42]. Bcl-x_L favors the open configuration of VDAC [39], which is necessary for the movement of metabolic anions across the OMM [40]. Adding recombinant Bcl-x_L protein to isolated mitochondria allows metabolite exchange such as ADP across the outer membrane by inhibiting VDAC1 closure under conditions promoting its closed configuration [39]. Therefore, Bcl-x_L deficiency could limit metabolite crossing of the OMM and thereby reduce mitochondrial capacity. The reduced mitochondrial superoxide production rather reflects the reduced mitochondrial respiration under basal conditions.

We conclude that Bcl-x_L influences the mitochondrial morphology and affects cellular energy metabolism. *Bcl-x* gene knockout and subsequent deficiency of Bcl-x_L protein expression impairs OXPHOS and ETS capacity, but increases the activity of the pentose phosphate pathway and increases total cellular glutathione content to compensate for increased oxidative stress.

Conflict of interest

None.

Acknowledgment

This work was supported by the Deutsche Forschungsgemeinschaft (SFB1080 A10 and ME1922/16-1). We appreciate the continuous support by the IMB Core Facility Microscopy and thank Cheryl Ernest and Nicola B. Hamilton-Whitaker for excellent proofreading.

References

[1] S. Willis, C.L. Day, M.G. Hinds, D.C.S. Huang, The Bcl-2-regulated apoptotic pathway, J. Cell Sci. 116 (2003) 4053–4056, http://dx.doi.org/10.1242/jcs.00754.
[2] T. Kaufmann, S. Schlipf, J. Sanz, K. Neubert, R. Stein, C. Borner, Characterization of the signal that directs Bcl-x(L), but not Bcl-2, to the mitochondrial outer membrane, J. Cell Biol. 160 (2003) 53–64, http://dx.doi.org/10.1083/jcb.200210084.
[3] R. Chen, I. Valencia, F. Zhong, K.S. McColl, H.L. Roderick, M.D. Bootman, et al., Bcl-2 functionally interacts with inositol 1,4,5-trisphosphate receptors to regulate calcium release from the ER in response to inositol 1,4,5-trisphosphate, J. Cell Biol. 166 (2004) 193–203, http://dx.doi.org/10.1083/jcb.200309146.
[4] Y.-P. Rong, A.S. Aromolaran, G. Bultynck, F. Zhong, X. Li, K. McColl, et al., Targeting Bcl-2-IP3 receptor interaction to reverse Bcl-2's inhibition of apoptotic calcium signals, Mol. Cell 31 (2008) 255–265, http://dx.doi.org/10.1016/j.molcel.2008.06.014.
[5] G. Monaco, E. Decrock, H. Akl, R. Ponsaerts, T. Vervliet, T. Luyten, et al., Selective regulation of IP3-receptor-mediated Ca2+ signaling and apoptosis by the BH4 domain of Bcl-2 versus Bcl-Xl, Cell Death Differ. 19 (2012) 295–309, http://dx.doi.org/10.1038/cdd.2011.97.
[6] C. White, C. Li, J. Yang, N.B. Petrenko, M. Madesh, C.B. Thompson, et al., The endoplasmic reticulum gateway to apoptosis by Bcl-X(L) modulation of the InsP3R, Nat. Cell Biol. 7 (2005) 1021–1028, http://dx.doi.org/10.1038/ncb1302.
[7] G. Monaco, T. Vervliet, H. Akl, G. Bultynck, The selective BH4-domain biology of Bcl-2-family members: IP3Rs and beyond, Cell Mol. Life Sci. 70 (2013) 1171–1183, http://dx.doi.org/10.1007/s00018-012-1118-y.
[8] C.O. Eno, E.F. Eckenrode, K.E. Olberding, G. Zhao, C. White, C. Li, Distinct roles of mitochondria- and ER-localized Bcl-xL in apoptosis resistance and Ca2+ homeostasis, Mol. Biol. Cell 23 (2012) 2605–2618, http://dx.doi.org/10.1091/mbc.E12-02-0090.
[9] B. Westermann, Mitochondrial fusion and fission in cell life and death, Nat. Rev. Mol. Cell Biol. 11 (2010) 872–884, http://dx.doi.org/10.1038/nrm3013.
[10] S.B. Berman, Y.-B. Chen, B. Qi, J.M. McCaffery, E.B. Rucker, S. Goebbels, et al., Bcl-x L increases mitochondrial fission, fusion, and biomass in neurons, J. Cell Biol. 184 (2009) 707–719, http://dx.doi.org/10.1083/jcb.200809060.
[11] M.M. Cleland, K.L. Norris, M. Karbowski, C. Wang, D.-F. Suen, S. Jiao, et al., Bcl-2 family interaction with the mitochondrial morphogenesis machinery, Cell Death Differ. 18 (2011) 235–247, http://dx.doi.org/10.1038/cdd.2010.89.
[12] H. Li, Y. Chen, A.F. Jones, R.H. Sanger, L.P. Collis, R. Flannery, et al., Bcl-xL induces Drp1-dependent synapse formation in cultured hippocampal neurons, Proc. Natl. Acad. Sci. USA 105 (2008) 2169–2174, http://dx.doi.org/10.1073/pnas.0711647105.
[13] P. Delivani, C. Adrain, R.C. Taylor, P.J. Duriez, S.J. Martin, Role for CED-9 and Egl-1 as regulators of mitochondrial fission and fusion dynamics, Mol. Cell 21 (2006) 761–773, http://dx.doi.org/10.1016/j.molcel.2006.01.034.
[14] C. Sheridan, P. Delivani, S.P. Cullen, S.J. Martin, Bax- or Bak-induced mitochondrial fission can be uncoupled from cytochrome C release, Mol. Cell 31 (2008) 570–585, http://dx.doi.org/10.1016/j.molcel.2008.08.002.
[15] K.N. Alavian, H. Li, L. Collis, L. Bonanni, L. Zeng, S. Sacchetti, et al., Bcl-xL regulates metabolic efficiency of neurons through interaction with the mitochondrial F1FO ATP synthase, Nat. Cell Biol. 13 (2011) 1224–1233, http://dx.doi.org/10.1038/ncb2330.
[16] Y.-B. Chen, M.A. Aon, Y.-T. Hsu, L. Soane, X. Teng, J.M. McCaffery, et al., Bcl-xL regulates mitochondrial energetics by stabilizing the inner membrane potential, J. Cell Biol. 195 (2011) 263–276, http://dx.doi.org/10.1083/jcb.201108059.
[17] N. Arbel, D. Ben-Hail, V. Shoshan-Barmatz, Mediation of the antiapoptotic activity of Bcl-xL protein upon interaction with VDAC1 protein, J. Biol. Chem. 287 (2012) 23152–23161, http://dx.doi.org/10.1074/jbc.M112.345918.
[18] G. Monaco, E. Decrock, N. Arbel, A.R. van Vliet, R.M. La Rovere, H. De Smedt, et al., The BH4 domain of anti-apoptotic Bcl-XL, but not that of the related Bcl-2, limits the voltage-dependent anion channel 1 (VDAC1)-mediated transfer of pro-apoptotic Ca2+ signals to mitochondria, J. Biol. Chem. 290 (2015) 9150–9161, http://dx.doi.org/10.1074/jbc.M114.622514.
[19] M. Colombini, VDAC structure, selectivity, and dynamics, Biochim. Biophys. Acta 2012 (1818) 1457–1465, http://dx.doi.org/10.1016/j.bbamem.2011.12.026.
[20] H. Huang, X. Hu, C.O. Eno, G. Zhao, C. Li, C. White, An interaction between Bcl-xL and the voltage-dependent anion channel (VDAC) promotes mitochondrial Ca2+ uptake, J. Biol. Chem. 288 (2013) 19870–19881, http://dx.doi.org/10.1074/jbc.M112.448290.
[21] D. Pesta, E. Gnaiger, High-resolution respirometry: oxphos protocols for human cells and permeabilized fibers from small biopsies of human muscle, Methods Mol. Biol. 810 (2012) 25–58, http://dx.doi.org/10.1007/978-1-61779-382-0_3.
[22] T. Yoshida, A. Kakizuka, H. Imamura, BTeam, a novel BRET-based biosensor for the accurate quantification of ATP concentration within living cells, Sci. Rep. 6 (2016) 39618, http://dx.doi.org/10.1038/srep39618.
[23] T. Soucek, R. Cumming, R. Dargusch, P. Maher, D. Schubert, The Regulation of Glucose Metabolism by HIF-1 Mediates a Neuroprotective Response to Amyloid Beta Peptide, Neuron 39 (2003) 43–56.
[24] A. Pfeiffer, M. Jaeckel, J. Lewerenz, R. Noack, A. Pouya, T. Schacht, et al., Mitochondrial function and energy metabolism in neuronal HT22 cells resistant to oxidative stress, Br. J. Pharmacol. 171 (2014) 2147–2158, http://dx.doi.org/10.1111/bph.12549.
[25] L.J. Reitzer, B.M. Wice, D. Kennell, Evidence that glutamine, not sugar, is the major energy source for cultured HeLa cells, J. Biol. Chem. 254 (1979) 2669–2676.
[26] A. Herrero, G. Barja, Sites and mechanisms responsible for the low rate of free radical production of heart mitochondria in the long-lived pigeon, Mech. Ageing Dev. 98 (1997) 95–111.
[27] H.A. Lardy, D. Johnson, W.C. Mcmurray, Antibiotics as tools for metabolic studies. I. A survey of toxic antibiotics in respiratory, phosphorylative and glycolytic systems, Arch. Biochem. Biophys. 78 (1958) 587–597.
[28] P. Albrecht, J. Lewerenz, S. Dittmer, R. Noack, P. Maher, A. Methner, Mechanisms of oxidative glutamate toxicity: the glutamate/cystine antiporter system xc- as a neuroprotective drug target, CNS Neurol. Disord. Drug Targets 9 (2010) 373–382.
[29] K.C. Patra, N. Hay, The pentose phosphate pathway and cancer, Trends Biochem. Sci. 39 (2014) 347–354, http://dx.doi.org/10.1016/j.tibs.2014.06.005.
[30] A. Stincone, A. Prigione, T. Cramer, M.M.C. Wamelink, K. Campbell, E. Cheung, et al., The return of metabolism: biochemistry and physiology of the pentose phosphate pathway, Biol. Rev. Camb. Philos. Soc. 90 (2014) 927–963, http://dx.doi.org/10.1111/brv.12140.
[31] H. Kolbe, K. Keller, K. Lange, H. Herken, Metabolic consequences of drug-induced inhibition of the pentose phosphate pathway in neuroblastoma and glioma cells, Biochem. Biophys. Res. Commun. (1976), http://dx.doi.org/10.1016/0006-291X(76)90718-X.
[32] D.C. Liemburg-Apers, P.H.G.M. Willems, W.J.H. Koopman, S. Grefte, Interactions between mitochondrial reactive oxygen species and cellular glucose metabolism, Arch. Toxicol. 89 (2015) 1209–1226, http://dx.doi.org/10.1007/s00204-015-1520-y.
[33] J. Zhou, B.K. Deo, K. Hosoya, T. Terasaki, I.G. Obrosova, F.C. Brosius, et al., Increased JNK phosphorylation and oxidative stress in response to increased glucose flux through increased GLUT1 expression in rat retinal endothelial cells, Investig. Ophthalmol. Vis. Sci. 46 (2005) 3403–3410, http://dx.doi.org/10.1167/iovs.04-1064.
[34] I. Talior, M. Yarkoni, N. Bashan, H. Eldar-Finkelman, Increased glucose uptake promotes oxidative stress and PKC-delta activation in adipocytes of obese, insulin-resistant mice, Am. J. Physiol. Endocrinol. Metab. 285 (2003) E295–E302, http://dx.doi.org/10.1152/ajpendo.00044.2003.
[35] R.J. Youle, M. Karbowski, Mitochondrial fission in apoptosis, Nat. Rev. Mol. Cell Biol. (2005).
[36] R. Dringen, J. Hirrlinger, Glutathione pathways in the brain, Biol. Chem. 384 (2003) 505–516, http://dx.doi.org/10.1515/BC.2003.059.
[37] S. Shimizu, M. Narita, Y. Tsujimoto, Bcl-2 family proteins regulate the release of apoptogenic cytochrome c by the mitochondrial channel VDAC, Nature 399 (1999) 483–487, http://dx.doi.org/10.1038/20959.
[38] S. Shimizu, Y. Shinohara, Y. Tsujimoto, Bax and Bcl-xL independently regulate apoptotic changes of yeast mitochondria that require VDAC but not adenine nucleotide translocator, Oncogene 19 (2000) 4309–4318, http://dx.doi.org/10.1038/sj.onc.1203788.
[39] M.G. Vander Heiden, X.X. Li, E. Gottleib, R.B. Hill, C.B. Thompson, M. Colombini, Bcl-xL promotes the open configuration of the voltage-dependent anion channel and metabolite passage through the outer mitochondrial membrane, J. Biol. Chem. 276 (2001) 19414–19419, http://dx.doi.org/10.1074/jbc.M101590200.
[40] T. Hodge, M. Colombini, Regulation of metabolite flux through voltage-gating of VDAC channels, J. Membr. Biol. 157 (1997) 271–279.

[41] M.G. Vander Heiden, N.S. Chandel, X.X. Li, P.T. Schumacker, M. Colombini, C.B. Thompson, Outer mitochondrial membrane permeability can regulate coupled respiration and cell survival, Proc. Natl. Acad. Sci. USA 97 (2000) 4666–4671, http://dx.doi.org/10.1073/pnas.090082297.

[42] M.G. Vander Heiden, N.S. Chandel, P.T. Schumacker, C.B. Thompson, Bcl-xL prevents cell death following growth factor withdrawal by facilitating mitochondrial ATP/ADP exchange, Mol. Cell 3 (1999) 159–167.